




Research Article

CO₂ adsorption in hydrochar produced from waste biomass

Helida M. C. Fagnani¹  · Cleiser T. P. da Silva² · Murilo M. Pereira³ · Andrelson W. Rinaldi² · Pedro A. Arroyo¹ · Maria A. S. D. de Barros¹

© Springer Nature Switzerland AG 2019

Abstract

Sugar and ethanol plants produce a large amount of sugarcane bagasse. Such biomass can be the raw material for the production of an adsorbent to uptake CO₂. Thus, this work aimed to evaluate the hydrocarbonization of sugarcane bagasse and to study its use as a CO₂ adsorbent from a simulated flue gas. The temperature of the hydrothermal carbonization (HC) was set at 220 °C, while the operating time ranged from 12 to 48 h. Through the SEM–EDS analysis, the 48-h sample (HC48) was selected for chemical activation with KOH, resulting in activated hydrochar (AHC). The CO₂ and N₂ simple adsorption isotherms were obtained at 50, 70 and 80 °C. The results have shown a higher adsorption at a temperature of 50 °C for both gases. Activated hydrochar clearly preferred CO₂ instead of N₂ at 100 kPa as the maximum adsorption was 1.99 and 0.207 mmol g⁻¹, respectively. The highest selectivity of CO₂/N₂ was 12–50 °C, according to the “Ideal adsorbed solution theory” model. Therefore, AHC is clearly an eco-friendly adsorbent that can be used to minimize the resulting release of climate-damaging CO₂ from flue gas to atmosphere.

Keywords CO₂ adsorption · Purification of the flue gas · Hydrochar from sugarcane bagasse · Biomass residue for gas purification

1 Introduction

Large-scale ethyl alcohol production promoted the development of renewable energies related to the wastes of the sugarcane industry. This sector generates a huge amount of bagasse that is already used in heat and energy generation [1], in paper and pulp industries and in biochemical industries [2]. Bagasse can also be used as feedstock for the construction sector, animal food and furfural [2]. Other uses include bioelectricity and second-generation ethanol [2]. Nevertheless, bagasse production is much higher than its consumption, which justifies the research and development of new applications for it.

The Brazilian industrial scenario is based on boilers, which use air as a source of oxygen for burning and releasing of flue gas at atmospheric pressure, which is composed

of N₂ (85%) and CO₂ (15%) [3]. As CO₂ is a well-known greenhouse gas, its liberation into the environment should be avoided.

A promising technology used for the treatment of flue gas is adsorption. The removal efficiency through this process takes into account the physicochemical properties of each adsorbate. The nitrogen molecule has a kinetic diameter of 0.364 nm, while the carbon dioxide molecule is a fraction smaller (0.330 nm) [4]. Despite the similarities between both kinetic diameters, which would promote similar diffusion characteristics into adsorbent pores, the adsorption process can be influenced by the difference in the electronic property of each component. Note that the N₂ and CO₂ molecules have linear geometries but N₂ has a very short triple-bond nonpolar character, whereas CO₂ has a linear

✉ Helida M. C. Fagnani, helidamonique@gmail.com | ¹Department of Chemical Engineering, State University of Maringá, Av. Colombo 5790, Maringá, PR CEP 87020-900, Brazil. ²Laboratory of Materials Chemistry and Sensors - LMSen, State University of Maringá, Av. Colombo 5790, Maringá, PR CEP 87020-900, Brazil. ³University of Technology of Paraná – UTFPR, Rua Marçílio Dias 635, Apucarana, PR CEP 86812-460, Brazil.



geometry, nonpolar character, but, polar bonds. In addition, CO₂ also contains a large quadrupole moment that is capable of inducing specific interactions such as hydrogen bonding [4]. Such characteristics may strongly influence the adsorption process of such gases.

CO₂ released to the atmosphere from industrial processes may be minimized through adsorption. Adsorbents for such purpose include activated carbons, zeolites, MOFs and mesoporous silica. Activated carbons may be synthesized through a wide range of raw materials, including the ones from vegetal sources such as biomass wastes [5]. Spite biomass wastes have low costs, and some drawbacks are already present such as relatively low selectivity in operation. To overcome them, carbonization should be considered as a promising CO₂ adsorbent after some chemical modification that may provide higher alkalinity [6].

The bagasse is composed by cellulose fibers, lignin and hemicellulose [1]. With its lignocellulosic structure being constituted by macropores (diameter > 50 nm) [7], the sugarcane bagasse is considered as an excellent raw material for carbon.

Carbons may be obtained by pyrolysis or hydrothermal carbonation (HCT). The former occurs at high temperatures and forms the bio-oil linker, whereas the latter is carried out at lower temperatures and requires water as the solvent, which is compatible with eco-friendly routes [5]. The HCT process occurs in mild conditions (150–250 °C) and provides low CO₂ emissions [8, 9]. It is influenced not only by temperature and reaction time, but also by its raw material as well as to the ratio between biomass and water that is placed in the reactor [10].

Temperature is by far the most important parameter in the HTC process because it is related directly to the biomass conversion into products in the solid, liquid and gas phases [5, 8]. As temperature is inversely proportional to the solid production, the range of different liquid and gaseous products intensifies with higher temperatures. Generally, the solid product is dominant in the temperature ranges of 150–220 °C [8, 10]. Naturally, the influence of reaction time should not be neglected; it defines the composition of the product as well as the total biomass conversion until a certain period. After that, the time has no impact on the process [10]. The products differ in short and long times of reaction and in high and low temperatures; so these two parameters should be investigated simultaneously.

Unfortunately, hydrochar has a low surface area [11], a characteristic that is not desired for adsorption purposes. The correction of this deficiency can be made by the hydrochar activation [7, 12]. As a consequence of this activation, the lignocellulosic biomass is activated as well, resulting in the formation of highly porous activated

carbons, which are necessary for CO₂ removal from combustion processes [13].

The activation can be physically or chemically performed. The chemical activation always happens when the carbon is impregnated or mixed with a chemical activating agent [14], and subjected to a thermal treatment in an inert atmosphere (usually helium or argon gas). Among the activation agents, KOH promotes the formation of samples with high superficial areas with narrow pore distribution [11] and a larger number of functional groups [15]. Such features favor the attraction of CO₂ by the material at a sub-atmospheric pressure [16].

Adsorption in porous solids has been proposed as a viable alternative for the treatment of the flue gas [17–19]. However, in order to improve the efficiency of the adsorption process, the adsorbent should have not only a high adsorption capacity, but also a high selectivity [20] in addition to being easily regenerated [21]. The regeneration degree of the adsorbent can be determined by calculating its isosteric heat of adsorption [17].

Therefore, the present work aims to evaluate the HCT process of agro-industrial residue as a carbon source and to study its use as a CO₂ adsorbent. Due to the vast sugarcane industry in Brazil, bagasse was chosen as the raw material for carbonization purposes. Single gas adsorption of CO₂ and N₂ was carried out at different temperatures (50, 70 and 80 °C) and pressures up to 100 kPa. The simulated flue gas was investigated through the ideal adsorbed solution theory (IAST) [22]. CO₂/N₂ selectivity was predicted, while the isosteric heat of adsorption was calculated by the Clausius–Clapeyron method.

2 Materials and methods

2.1 Bagasse collect and storage

Sugarcane bagasse was kindly donated by an alcohol plant located in the northern region of Paraná, Brazil. As soon as the bagasse was collected, it was dried up in an oven at 50 °C for 2 days and sieved with a particle size of less than 0.841 mm. The sample was then stored in the absence of light and moisture.

2.2 Synthesis and characterization of hydrochars

The HTC reactions occurred in Teflon[®] reactors, externally coated by 30-mL stainless steel cylinders. In each reactor, 0.500 g of sugarcane bagasse was added to 20 mL of deionized water. The system was heated at a rate of 10 °C min⁻¹ up to 220 °C, and kept constant at this temperature for 12, 24, 36 and 48 h to produce the samples HC12, HC24, HC36 and HC48, respectively. After cooling

back to room temperature, the hydrochar samples were filtered, and oven dried at 105 °C for 5 h. The hydrochar synthesis was carried out in duplicates.

An energy dispersive X-ray spectrometer (EDS) was used for qualitative analysis, along with the scanning electron microscopy (SEM) in all hydrochar samples. The solid was gold sputter coating in the Quorum metallizer, model Q150RES. Subsequently, the samples were observed in the Zeiss model EVO/MAI 15.

The hydrochar with the highest carbon concentration was submitted to activation and underwent textural characterization and infrared spectroscopy analysis by attenuated total reflectance (ATR–FTIR). ATR–FTIR analysis was carried out in the Varian 700 FTIR spectrometer with a germanium crystal in the range of 4000–700 cm^{-1} with a resolution of 2 cm^{-1} . The textural characterization was performed using Micromeritics equipment, model ASAP 2020. First, a vacuum pre-treatment of 10^{-3} kPa was done for 4 h at a temperature of 300 °C. Secondly, the sample was exposed to N_2 adsorption/desorption. Measurements were performed at 77 K.

2.3 Activation of hydrochar

The activation of the selected sample was based on the methodology described elsewhere [15]. Two grams of the selected hydrochar sample were added to 250 mL of a 40 g L^{-1} KOH solution. The suspension was stirred for 10 min on a magnetic stirrer, heated to 150 °C, and maintained at this temperature until the volume was reduced to 10 mL. Then, a reactor was used with an argon flow rate of 500 mL min^{-1} , and the system was heated at a rate of 25 $^{\circ}\text{C min}^{-1}$ up to 800 °C and kept at this temperature for 45 min. After being cooled down to room temperature, the activated hydrochar (AHC) sample was washed three times with 200 mL of deionized water and finally, oven dried for 12 h at a temperature of 120 °C.

The AHC sample was also analyzed by textural characterization (nitrogen adsorption/desorption isotherm) and ATR–FTIR analysis.

2.4 Adsorption in the activated hydrochar

The AHC sample was used in single adsorption of CO_2 (purity 99.99%) and N_2 (purity 99.999%). As the usual temperature of flue gas is around 50 °C [16], adsorption isotherms were obtained at 50, 70 and 80 °C. The latter two temperatures were investigated to predict a breakdown in the downstream cooling system. Temperatures higher than 80 °C were not presented herein because preliminary results indicated a negligible adsorption capacity of both gases. Micromeritics brand ASAP 2020 equipment was used to carry low partial pressure (up

to 100 kPa) isotherms. The experimental procedure followed the manual instructions of the equipment. Temperature accuracy was ± 0.1 °C. A brief description includes sample treatment and the gas adsorption. Firstly, sampling was performed under a vacuum of 10^{-3} kPa for 4 h at 300 °C. At this point, the treated sample was exposed to a stream of CO_2 or N_2 gas with a pressure ranging from 0.1 to 100 kPa (P_0) to perform the adsorption isotherm. The adsorption models of Langmuir (Eq. 1) [23] and Sips (Eq. 2) [24] were used to represent experimental data.

$$q_{\text{eq}} = \frac{q_{\text{max}} \cdot b \cdot P}{1 + b \cdot P} \quad (1)$$

$$q_{\text{eq}} = \frac{q_{\text{max}} \cdot (b \cdot P)^{1/n}}{1 + (b \cdot P)^{1/n}} \quad (2)$$

where q_{eq} is the amount adsorbed; q_{max} is the saturation capacity; P is the gas phase pressure; b is a constant, and n is a parameter representing the system heterogeneity.

The CO_2 selectivity of the CO_2/N_2 binary mixture is presented in Eq. 3 [17] where x refers to the molar fraction in the adsorbed phase, and y refers to the molar fraction in the gas phase. The value of x was estimated by the ideal adsorbed solution theory (IAST), which developed by Myers and Prausnitz [22], is widely accepted [25].

$$S_{1/2} = \frac{x_1/x_2}{y_1/y_2} \quad (3)$$

2.5 Isotheric heat of adsorption

In order to calculate the isotheric heat of adsorption, a Clausius–Clapeyron method [26] was used, with an adsorbed amount of isotherms obtained at low pressures, as represented in Eq. 4:

$$Q_{\text{ST}} = -R \left[\frac{\partial(\ln P)}{\partial\left(\frac{1}{T}\right)} \right]_{n_a} \quad (4)$$

where n_a is the specific amount adsorbed at a pressure P (bar) and temperature T (K). A plot of $\ln P$ against $1 \cdot T^{-1}$ gives a straight line whose slope represents Q_{ST}/R , in which Q_{ST} is the isotheric heat of adsorption (J mol^{-1}) and R is a gas constant ($\text{J mol}^{-1} \text{K}^{-1}$). For the calculation of the isotheric heat, different amounts of adsorbed CO_2 and N_2 were used in the AHC, in the range of zero to the highest adsorption capacity for each gas in the three temperatures investigated [27].

3 Results and discussion

3.1 Activated hydrochar production

As hydrocarbonization proceeds, hydrogen and oxygen compounds are released to the aqueous environment, while the solid phase becomes richer in carbon [11], which consequently explains the decreasing content of hydrogen and oxygen as the hydrocarbonization continues (Fig. 1) [1]. In conclusion, time is extremely important in the hydrochar synthesis; hence, the hydrochar of 48 h (HC48) had the highest amount of carbon (70.94%) and lower yield mass (40.13%), which are close to the previously reported results [28].

As expected, scanning electron microscopy (SEM) was able to provide clear distinction in the original biomass when compared to the hydrochar samples, as shown in Fig. 2. As samples are coated with a thin layer of gold, the micropores are not visible in the SEM images. However, adsorption/desorption isotherms of N_2 demonstrates that the AHC sample has microporous characteristics. It also highlights the presence of microspheres or irregular particles, which is a consequence of the low hydrocarbonization temperature [29] that is associated with a range of distinct functional groups such as carbonyl, hydroxyl, carboxylic, ester, and quinone [9]. These structures are more often present in higher running times of hydrocarbonization [1]. This is exemplified by the hydrochar sample obtained at 48 h (HC48) (Fig. 2e), where more disruption of the cellulose molecules in the raw biomass material had probably occurred.

According to the EDS and SEM analysis, the HC48 was chosen as the best sample to be activated and used in

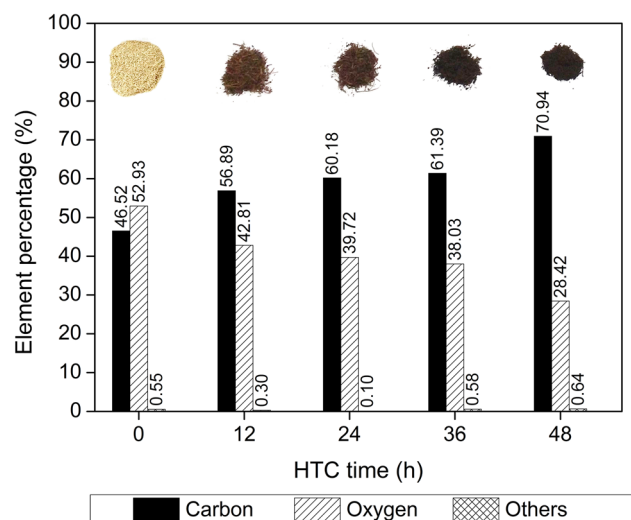


Fig. 1 Energy dispersive X-ray spectrometer

adsorption. The mass yield of the activation was 17.23%, in other words, the total mass yield of the hydrochar production and activation process was 6.91%.

Following this, HC48 and its activated form, AHC, were submitted to characterization. The adsorption/desorption N_2 isotherm at 77 K of both samples is shown in Fig. 3. The pore distribution is shown in Fig. 4. The adsorption/desorption isotherm of HC48 (Fig. 3a) is classified as type IV, which is a characteristic of mesoporous materials [30]. As expected, the pore distribution of HC48, as shown in Fig. 4a, has a wide range of large pore diameters, with an average pore diameter of 28.3 nm as estimated by the Barrett–Joyner–Halenda (BJH) method. Nevertheless, the AHC isotherm (Fig. 3b) is classified as type I(b), which indicates that the material has a pore size distribution in the range of larger micropores and possibly narrow mesopores, which can be observed in the pore distribution (Fig. 4b). Pores measuring below 1.0 nm and pores between 1.0 and 4.0 nm can be observed. This fact is in agreement with results already reported by [31, 32]. The specific surface area calculated by the BET method of HC48 and AHC samples is $13 \text{ m}^2 \text{ g}^{-1}$ and $2080 \text{ m}^2 \text{ g}^{-1}$, respectively. The HC48 pore volume is $0.0941 \text{ cm}^3 \text{ g}^{-1}$, in which only $0.0101 \text{ cm}^3 \text{ g}^{-1}$ is of micropores, whereas for the AHC, the volume of micropores is $1.246 \text{ cm}^3 \text{ g}^{-1}$ of the total of $1.316 \text{ cm}^3 \text{ g}^{-1}$. Due to the significant increase in the specific surface area and microporosity, the AHC may be successfully used in adsorption.

According to the ATR–FTIR analysis of the HC48 and AHC, as shown in Fig. 5, the characteristic bands of sugarcane bagasse, such as cellulose (900 cm^{-1} deformation of C–H), hemicellulose (1163 cm^{-1} C–O–C vibration) and lignin (region of $1000\text{--}1500 \text{ cm}^{-1}$) [9], are observed in the HC48 sample, although they are not seen in the AHC sample. There was disruption of the remaining structures during activation for the formation of pores, also reported in the spectrum [12]. Moreover, there was the detection of more intense bands in the region of $1800\text{--}2800 \text{ cm}^{-1}$ in HC48, suggesting the break of chemical bonds during the activation process. This fact occurs mainly due to the rupture of the spherical morphology present in the HC48 [9]. However, the bands 2920 cm^{-1} and 2830 cm^{-1} are present in both HC48 and AHC and are attributed to the C–H vibration elongation of carboxylic acids [12, 33]. Yet, the band at 1640 cm^{-1} in HC48 is related to the elongation vibration of the C=O in the carbonyl [12]; this band decreased in intensity and suffered displacement in AHC. The 1026 cm^{-1} band seen in the AHC sample is attributed to elongation of the C–O–C bonds, which may be present in esters [33] and had its intensity increased after activation. Finally, samples of HC48 and AHC contain a band between 3000 and 3600 cm^{-1} bands, which are attributed to the O–H stretching vibrations in hydroxyl or carboxylic groups [34,

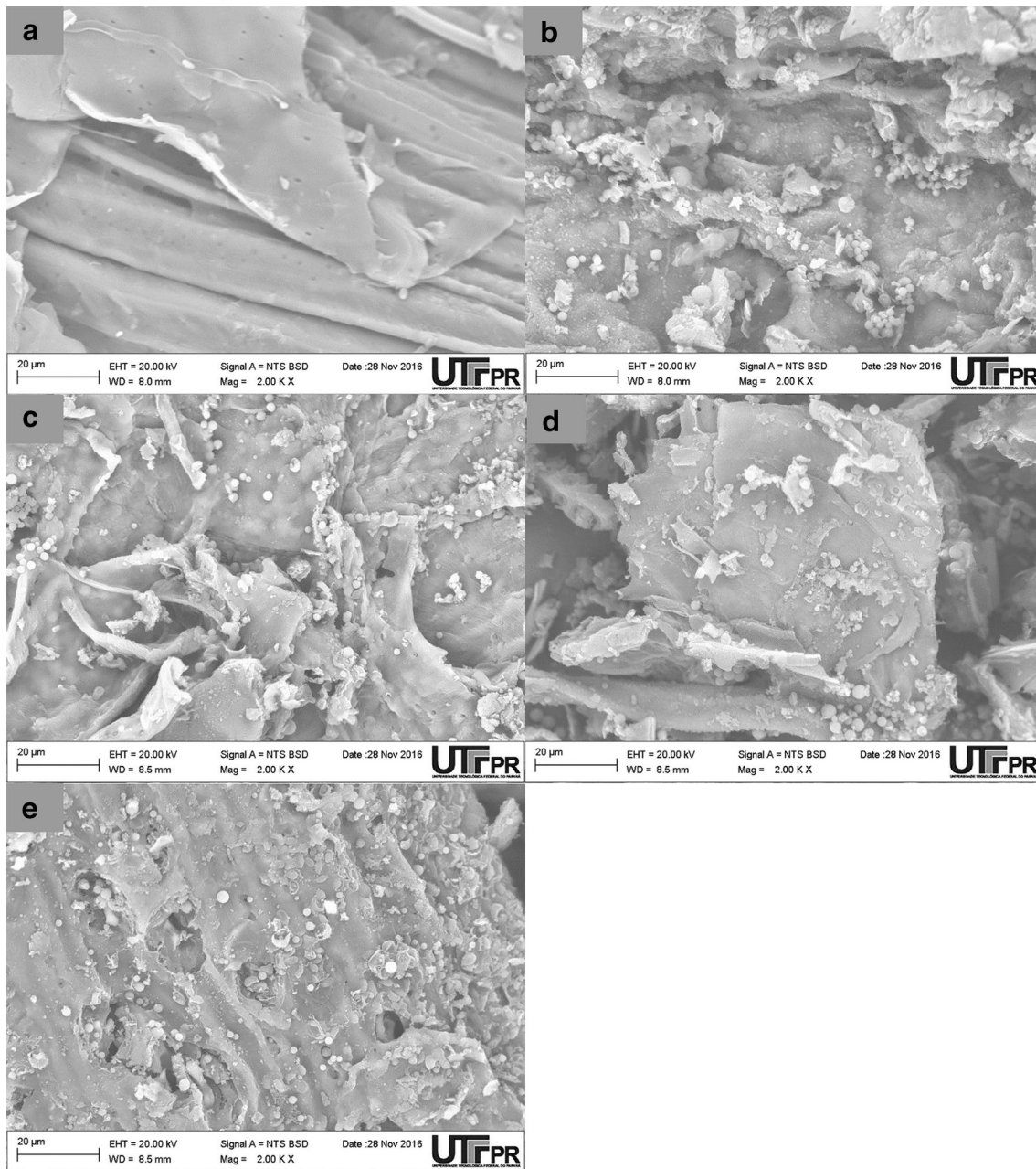


Fig. 2 Scanning electron spectroscopy: **a** in sugarcane bagasse; and hydrochars of: **b** 12 h; **c** 24 h; **d** 36 h; **e** 48 h

35], are also seen in the KOH spectrum [36]. Such group allows the adsorption of acidic compounds in the material such as CO_2 . Moreover, AHC has a high surface area with pronounced microporosity and narrow mesopores. These features may also contribute to CO_2 adsorption [16].

3.2 Gas adsorption and selectivity

The adsorption isotherms are presented in Fig. 6. In analyzing those isotherms, it comes to the conclusion that at the lowest temperature of 50 °C, it had the highest amount

of adsorption over the whole pressure range. In this way, agreeing with previous works where physisorption is the predominant mechanism in gas adsorption [16].

The adsorption of CO_2 in the AHC was higher than N_2 . At the conditions of 50 °C and 100 kPa, the adsorption capacity was 1.99 mmol g^{-1} and 0.207 mmol g^{-1} of CO_2 and N_2 , respectively. Discrepancies in the adsorption capacity are a consequence of the differences in physicochemical properties of the gaseous phase. Indeed, the quadrupole moment of CO_2 is responsible for the electrostatic interactions of such molecules with the basic Lewis sites present

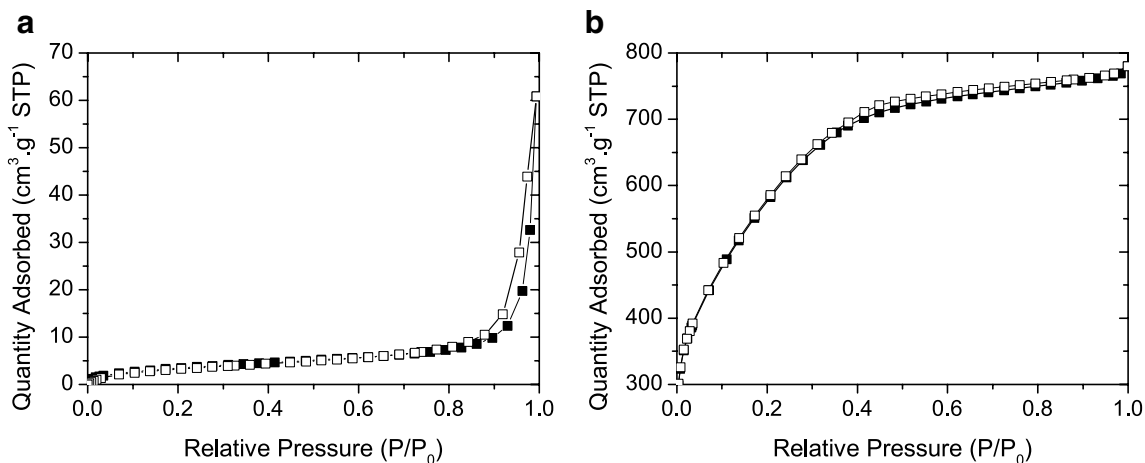


Fig. 3 Isotherms of adsorption/desorption of N₂ of **a** HC48; **b** AHC

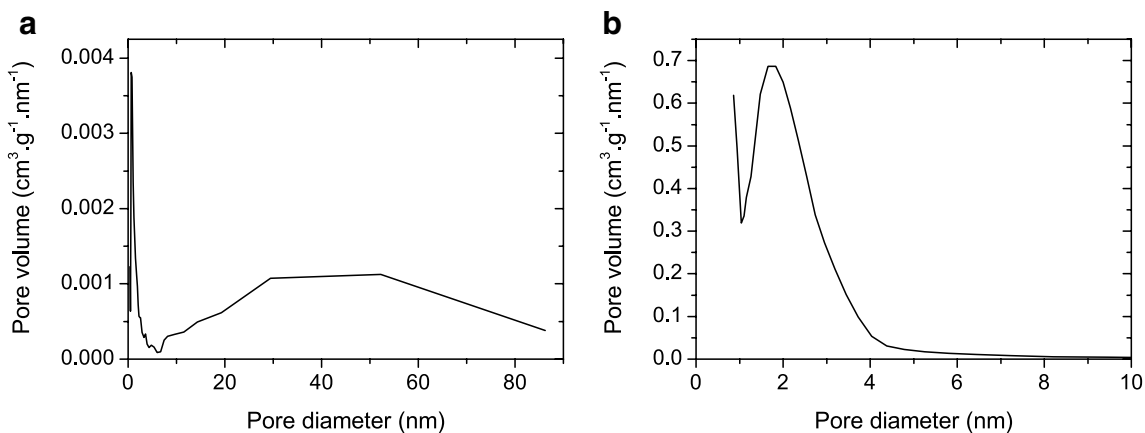


Fig. 4 Pore size distribution of: **a** HC48; **b** AHC

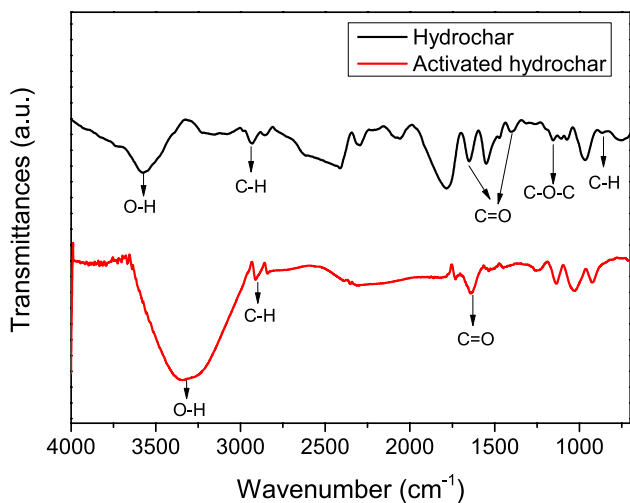


Fig. 5 ATR-FTIR of HC48 and AHC

on the AHC surface (mainly OH⁻). On the other hand, the nonpolar nitrogen molecule is less attracted to the superficial groups of activated hydrochar.

By means of the monocomponent adsorption isotherms at the three different temperatures investigated herein, the isosteric adsorption heat (Q_{ST}) was calculated. Results are present in Fig. 7. The equilibrium amount varied from 0.04 up to 0.80 mmol g⁻¹ for CO₂, whereas values between 0.004 and 0.088 mmol g⁻¹ were observed for N₂. It is seen that the Q_{ST} value decreases with increasing uptake amount, which may be related to the heterogeneity of adsorption sites (based on the theory of the Langmuir isotherm model). In addition, at the beginning of the adsorption, there are a large number of vacant pores on the surface of the AHC. So the CO₂ and N₂ molecules interact directly with the adsorbent surface through van der Waals forces. As the pores are filled, the

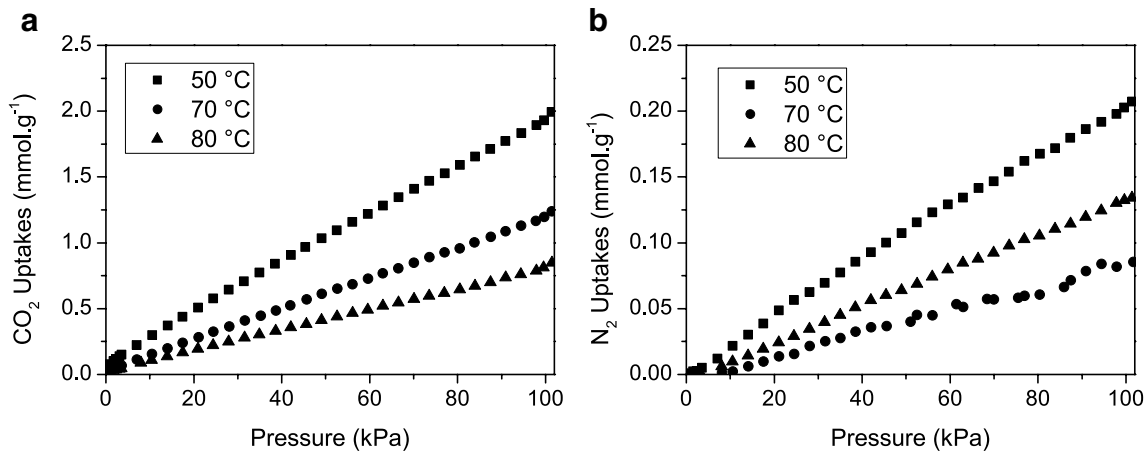


Fig. 6 Adsorption isotherms at different temperatures of: **a** CO₂; **b** N₂

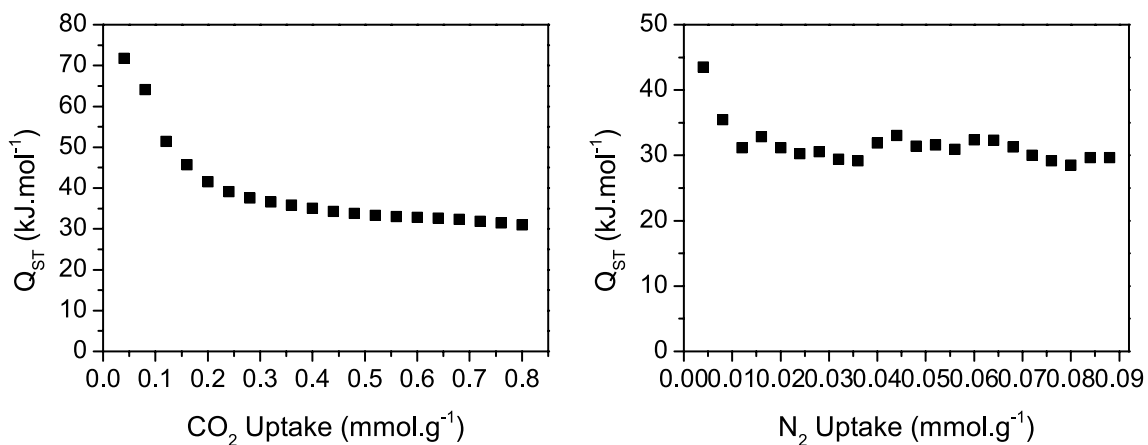


Fig. 7 Isothermic adsorption heat of CO₂ and N₂ in AHC

van der Waals force decreases. As a consequence, the isosteric adsorption heat reduces [27]. The mean value of Q_{ST} for was between 38 and 39 kJ mol⁻¹ for CO₂, which is in agreement with previous results [3, 35]. Q_{ST} values in the range of 30–31 kJ mol⁻¹ were estimated for N₂ molecules. In both the cases, the exothermic behavior of the physisorption process was verified [37]. The higher the value of Q_{ST} , the stronger is the interaction between the gas and the AHC. Therefore, the isosteric adsorption heat shows the selectivity CO₂ > N₂. In fact, this result was already expected due to the physicochemical characteristics of the adsorbates previously mentioned in characterized AHC.

The isosteric adsorption heat values estimated in this paper were slightly higher than those already reported [3] for CO₂ and N₂ adsorbed in activated carbon. However, the values are still low, suggesting that a physical adsorption occurs [38], in order to allow the adsorbent to regenerate [21].

To predict the adsorption equilibrium behavior of the gases over a wide temperature and pressure range, the Langmuir and Sips adsorption models were used (Fig. 8). The parameter adjustments to the experimental data are in Table 1 for Langmuir and Table 2 for Sips models. Although the Langmuir model was the one with the highest R^2 and the lowest χ^2 for the adsorption of CO₂, the Sips model was the best fit for N₂ adsorption data in AHC. The N₂ adsorption isotherm at 80 °C was poorly represented by both models, due to its low adsorption capacity.

IAST methodology was used to predict the selectivity of CO₂/N₂ for the flue gas (15/85 vol%) at steady temperatures, along with pressure ranging from 0 to 100 kPa. Results are shown in Fig. 9. The CO₂ isotherms were adjusted to the Langmuir model, whereas N₂ used the Sips model.

In all temperatures, the CO₂/N₂ selectivity was higher at low pressures and decreased to a close constant selectivity

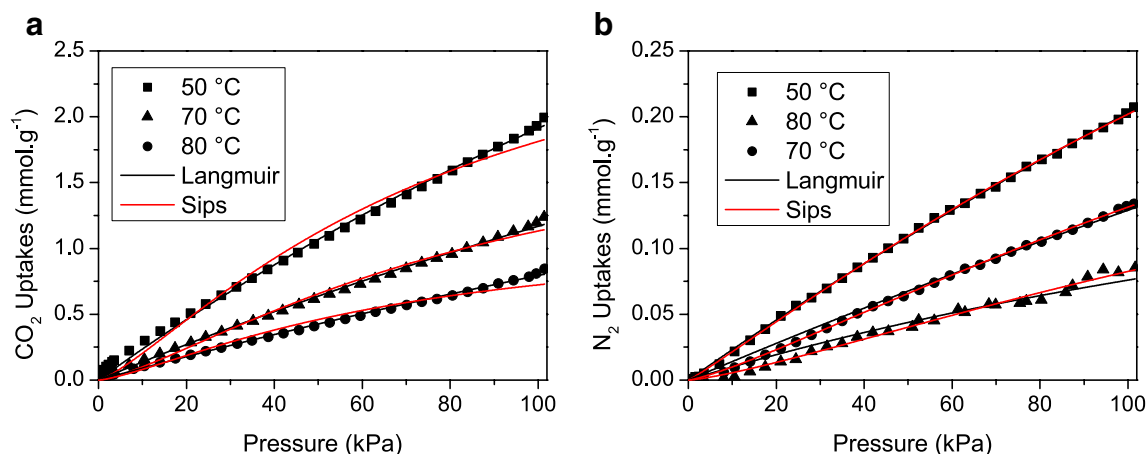


Fig. 8 Adjustment of the Langmuir and Sips models at the temperatures of 50, 70 and 80 °C for the gas: **a** CO₂; **b** N₂

Table 1 Parameters obtained for the adjustment of the Langmuir model in the adsorption of CO₂ and N₂ at different temperatures

Gas	Temp. (°C)	q_{max} (mmol · g ⁻¹)	b (kPa ⁻¹) (10 ⁻⁴)	R^2	χ^2 (10 ⁻⁶)
CO ₂	50	9.146 ± 0.9760	26.46 ± 3.393	0.9970	1220
	70	6.944 ± 0.7900	20.22 ± 2.659	0.9981	309.8
	80	5.829 ± 0.9029	15.77 ± 2.742	0.9977	165.0
N ₂	50	1.483 ± 0.1097	15.85 ± 1.315	0.9995	2.467
	70	1.384 ± 0.4885	10.27 ± 3.917	0.9944	9.752
	80	0.2855 ± 0.09146	36.34 ± 14.76	0.9590	28.55

Table 2 Parameters obtained for the adjustment of the Sips model in the adsorption of CO₂ and N₂ at different temperatures

Gas	Temp. (°C)	q_{max} (mmol · g ⁻¹)	b (kPa ⁻¹) (10 ⁻³)	n	R^2	χ^2 (10 ⁻⁶)
CO ₂	50	3.133 ± 0.5243	12.71 ± 3.334	0.7721 ± 0.08213	0.9873	5200
	70	2.108 ± 0.4449	10.68 ± 3.211	0.7336 ± 0.08168	0.9875	2010
	80	1.445 ± 0.3342	10.42 ± 3.441	0.7403 ± 0.08768	0.9857	1040
N ₂	50	0.8250 ± 0.09429	3.535 ± 0.5610	0.9233 ± 0.01924	0.9996	1.761
	70	0.4746 ± 0.05529	4.641 ± 0.6721	0.7997 ± 0.01962	0.9994	1.046
	80	0.2897 ± 0.1516	4.942 ± 3.084	0.7660 ± 0.08523	0.9880	8.388

of 12 from 40 up to 100 kPa. At low pressures, the competition to adsorption sites is negligible. In this case, AHC strongly prefers CO₂ molecule due to the quadrupole–dipole interaction between gas–solid. This fact can also be related to isosteric adsorption heat (Fig. 7). In such condition, heat reaches higher values for both gases. From 40 to 100 kPa, at 70 and 80 °C, selectivity remains in the ratio of 12 molecules of CO₂ to 1 molecule of N₂. That is, after filling the first adsorbent sites, the uptake amount of CO₂ gas decreases relative to the uptake amount of N₂ gas. With increasing pressure, N₂ molecules are pushed to the adsorption sites. Thus, the chemical structure of the molecule has minor influence in the equilibrium of adsorption. This fact is also observed in the isosteric adsorption heat (Fig. 7). The CO₂ isosteric heat decreases as the adsorption occurs, whereas the N₂ remains almost constant. At 50 °C, the selectivity increases slowly, but the average is also

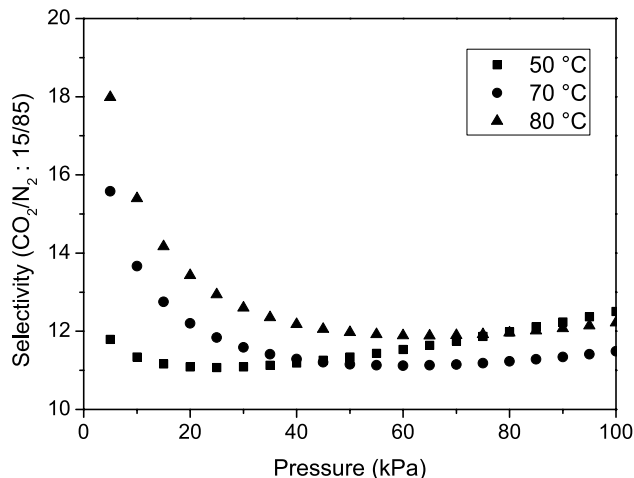


Fig. 9 CO₂/N₂ selectivity for the combustion gas calculated by IAST at the different test temperatures

Table 3 CO₂/N₂ selectivity of the flue gas found in the literature

Adsorbent	Temp. (°C)	Pressure (kPa)	CO ₂ uptake (mmol g ⁻¹)	Selectivity	References
Activated carbon honeycomb monolith	26	100	2.5	6.5	[3]
Activated hydrochar of sawdust	25	100	4.8	5.4	[32]
Nanostructured templated carbon by tuning surface area and nitrogen doping	25	101.3	4.0	6.1	[39]
Ordered mesoporous carbon	25	100	3.0	10	[21]
Activated microporous carbon compartments	25	100	3.5	16	[19]
Magnetic activated lignin from eucalyptus and spruce	50	100	4.0	3.2	[40]
Carbon monoliths	47	105	3.0	12	[18]
Palm kernel shell-based activated carbon	25	101.3	2.1	7.0	[27]
Nitrogen-doped biocarbons derived from rotten strawberries	25	100	4.3	16	[41]
Activated hydrochar of sugarcane bagasse	50	100	2.0	12	This paper

close to 12 molecules of CO₂ to 1 molecule of N₂. Results reported in the literature of CO₂/N₂ selectivity of the flue gas in carbon are presented in Table 3.

The major advantage of the hydrochar here investigated is higher when compared to many other activated carbons and hydrochars (Table 3) or as large as Querejeta et al. [18]. Therefore, hydrochars from sugarcane bagasse are a promising adsorbent for CO₂ removal, specifically, when it comes to the purification of the flue gas.

4 Conclusions

In this paper, activated hydrochar was obtained from sugarcane bagasse through an eco-friendly route. The best HC sample was obtained after 48 h. Its activated sample (AHC) generated a microporous material with high specific surface area and important alkaline superficial groups such as hydroxide, responsible for the retention of the acid gas CO₂.

Physisorption seems to be the preferred removal mechanism with the lowest temperature of 50 °C. The isosteric adsorption heat of CO₂ was 77.10 kJ mol⁻¹ and N₂ of 30.89 kJ mol⁻¹. These values are in agreement with such mechanism. AHC has much more affinity to CO₂ than to N₂, and the CO₂/N₂ selectivity was estimated at 12 according to the IAST model.

According to results presented herein, AHC is a proven CO₂ adsorbent that can be efficiently used to minimize the greenhouse effects.

Compliance with ethical standards

Conflict of interest On behalf of all authors, the corresponding author states that there is no conflict of interest.

References

- Iryani DA, Kumagai S, Nonaka M, Sasaki K, Hirajima T (2017) Characterization and production of solid biofuel from sugarcane bagasse by hydrothermal carbonization. *Waste Biomass Valoriz* 8:1941–1951. <https://doi.org/10.1007/s12649-017-9898-9>
- Anukam A, Mamphweli S, Reddy P, Meyer E, Okoh O (2016) Pre-processing of sugarcane bagasse for gasification in a downdraft biomass gasifier system: a comprehensive review. *Renew Sustain Energy Rev* 66:775–801. <https://doi.org/10.1016/j.rser.2016.08.046>
- Ribeiro RP, Sauer TP, Lopes FV, Moreira RF, Grande CA, Rodrigues AE (2008) Adsorption of CO₂, CH₄, and N₂ in activated carbon honeycomb monolith. *J Chem Eng Data* 53:2311–2317. <https://doi.org/10.1016/j.jee.2016.09.001>
- Shriver DF, Atkins PW (2008) *Química inorgânica*. Bookman, Porto Alegre
- Kambo HS, Minaret J, Dutta A (2018) Process water from the hydrothermal carbonization of biomass: a waste or a valuable product? *Waste Biomass Valoriz* 9:1181–1189. <https://doi.org/10.1007/s12649-017-9914-0>
- Yu CH, Huang CH, Tan CS (2012) A review of CO₂ capture by absorption and adsorption. *Aerosol Air Qual Res* 12:745–769. <https://doi.org/10.4209/aaqr.2012.05.0132>
- Rattanachueskul N, Saning A, Kaowphong S, Chumha N, Chuenchom L (2017) Magnetic carbon composites with a hierarchical structure for adsorption of tetracycline, prepared from sugarcane bagasse via hydrothermal carbonization coupled with simple heat treatment process. *Bioresour Technol* 226:164–172. <https://doi.org/10.1016/j.biortech.2016.12.024>
- Lohri CR, Zabaleta I, Rohr M, Baier U, Zurbrugg C (2018) Improving the energy-related aspects of biowaste treatment in an experimental hydrothermal carbonization reactor. *Waste Biomass Valoriz* 9:429–442. <https://doi.org/10.1007/s12649-016-9746-3>
- Sevilla M, Maciá-Agulló JA, Fuertes AB (2011) Hydrothermal carbonization of biomass as a route for the sequestration of CO₂: chemical and structural properties of the carbonized products. *Biomass Bioenergy* 35:3152–3159. <https://doi.org/10.1016/j.biombioe.2011.04.032>
- Nizamuddin S, Baloch HA, Griffin GJ, Mubarak NM, Bhutto AW, Abro R, Mazari SA, Ali BS (2017) An overview of effect of process parameters on hydrothermal carbonization of biomass. *Renew Sustain Energy Rev* 73:1289–1299. <https://doi.org/10.1016/j.rser.2016.12.122>

11. Jain A, Balasubramanian R, Srinivasan MP (2016) Hydrothermal conversion of biomass waste to activated carbon with high porosity: a review. *Chem Eng J* 283:789–805. <https://doi.org/10.1016/j.cej.2015.08.014>
12. Li M, Li W, Liu S (2011) Hydrothermal synthesis, characterization, and KOH activation of carbon spheres from glucose. *Carbohydr Res* 346:999–1004. <https://doi.org/10.1016/j.carres.2011.03.020>
13. Sevilla M, Fuertes AB, Mokaya R (2011) High density hydrogen storage in superactivated carbons from hydrothermally carbonized renewable organic materials. *Energy Environ Sci* 4:1400–1410. <https://doi.org/10.1039/c0ee00347f>
14. Libra J, Kyoung SR, Kammann C, Funke A, Berge N, Neubauer Y, Titirici M, Fühner C, Bens O, Kern J, Emmerich K-H (2011) Hydrothermal carbonization of biomass residuals: a comparative review of the chemistry, processes and applications of wet and dry pyrolysis. *Biofuels* 2:89–124. <https://doi.org/10.4155/BFS.10.81>
15. Li Y, Ruan G, Jalilov AS, Tarkunde YR, Fei H, Tour JM (2016) Biochar as a renewable source for high-performance CO₂ sorbent. *Carbon N Y* 107:344–351. <https://doi.org/10.1016/j.carbon.2016.06.010>
16. Plaza MG, González AS, Pis JJ, Rubiera F, Pevida C (2014) Production of microporous biochars by single-step oxidation: effect of activation conditions on CO₂ capture. *Appl Energy* 114:551–562. <https://doi.org/10.1016/j.apenergy.2013.09.058>
17. Álvarez-Gutiérrez N, Gil MV, Rubiera F, Pevida C (2016) Adsorption performance indicators for the CO₂/CH₄ separation: application to biomass-based activated carbons. *Fuel Process Technol* 142:361–369. <https://doi.org/10.1016/j.fuproc.2015.10.038>
18. Querejeta N, Plaza MG, Rubiera F, Pevida C, Avery T, Tennisson SR (2017) Carbon monoliths in adsorption-based post-combustion CO₂ capture. *Energy Procedia* 114:2341–2352. <https://doi.org/10.1016/j.egypro.2017.03.1366>
19. Hong S-M, Jang E, Dysart AD, Pol VG, Lee KB (2016) CO₂ Capture in the sustainable wheat-derived activated microporous carbon compartments. *Sci Rep* 6:1–10. <https://doi.org/10.1038/srep34590>
20. Das SK, Wang X, Ostwal MM, Lai Z (2016) A highly stable microporous covalent imine network adsorbent for natural gas upgrading and flue gas CO₂ capture. *Sep Purif Technol* 170:68–77. <https://doi.org/10.1016/j.seppur.2016.06.016>
21. Yuan B, Wu X, Chen Y, Huang J, Luo H, Deng S (2013) Adsorption of CO₂, CH₄, and N₂ on ordered mesoporous carbon: approach for greenhouse gases capture and biogas upgrading. *Environ Sci Technol* 47:5474–5480. <https://doi.org/10.1021/es4000643>
22. Myers AL, Prausnitz JM (1965) Thermodynamics of mixed-gas adsorption. *AIChE J* 11:121–127. <https://doi.org/10.1002/aic.690110125>
23. Langmuir I (1918) The adsorption of gases on plane surfaces of glass, mica and platinum. *J Am Chem Soc* 40:1361–1403. <https://doi.org/10.1021/ja02242a004>
24. Sips R (1948) Combined form of Langmuir and Freundlich equations. *J Chem Phys* 16:490–495. <https://doi.org/10.1063/1.1746922>
25. Islamoglu T, Behera S, Kahveci Z, Tessema T-D, Jena P, El-Kaderi HM (2016) Enhanced carbon dioxide capture from landfill gas using bifunctionalized benzimidazole-linked polymers. *ACS Appl Mater Interfaces* 8:14648–14655. <https://doi.org/10.1021/acsami.6b05326>
26. Pan H, Ritter JA, Balbuena PB (1998) Examination of the approximations used in determining the isosteric heat of adsorption from the Clausius–Clapeyron equation. *Langmuir* 14:6323–6327
27. Rashidi NA, Yusup S (2017) Potential of palm kernel shell as activated carbon precursors through single stage activation technique for carbon dioxide adsorption. *J Clean Prod* 168:474–486. <https://doi.org/10.1016/j.jclepro.2017.09.045>
28. Fang J, Gao B, Chen J, Zimmerman AR (2015) Hydrochars derived from plant biomass under various conditions: characterization and potential applications and impacts. *Chem Eng J* 267:253–259. <https://doi.org/10.1016/j.cej.2015.01.026>
29. Wang Q, Li H, Chen L, Huang X (2002) Novel spherical microporous carbon as anode material for Li-ion batteries. *Solid State Ion* 153:43–50. [https://doi.org/10.1016/S0167-2738\(02\)00687-2](https://doi.org/10.1016/S0167-2738(02)00687-2)
30. Thommes M, Kaneko K, Neimark AV, Olivier JP, Rodriguez-Reinoso F, Rouquerol J, Sing KSW (2015) Physisorption of gases, with special reference to the evaluation of surface area and pore size distribution (IUPAC technical report). *Pure Appl Chem* 87:1051–1069. <https://doi.org/10.1515/pac-2014-1117>
31. Falco C, Marco-Lozar JP, Slinas-Torres D, Morallón E, Cazorla-Amorós D, Titirici MM, Lozano-Castelló D (2013) Tailoring the porosity of chemically activated hydrothermal carbons: influence of the precursor and hydrothermal carbonization temperature. *Carbon N Y* 62:346–355. <https://doi.org/10.1016/j.carbon.2013.06.017>
32. Sevilla M, Fuertes AB (2011) Sustainable porous carbons with a superior performance for CO₂ capture. *Energy Environ Sci* 4:1765–1771. <https://doi.org/10.1039/C0EE00784F>
33. Heidari A, Younesi H, Rashidi A, Ghoreyshi A (2014) Adsorptive removal of CO₂ on highly microporous activated carbons prepared from *Eucalyptus camaldulensis* wood: effect of chemical activation. *J Taiwan Inst Chem Eng* 45:579–588. <https://doi.org/10.1016/j.jtice.2013.06.007>
34. Reza MT, Rottler E, Herklotz L, Wirth B (2015) Hydrothermal carbonization (HTC) of wheat straw: influence of feedwater pH prepared by acetic acid and potassium hydroxide. *Bioresour Technol* 182:336–344
35. Volpe M, Goldfarb JL, Fiori L (2018) Hydrothermal carbonization of *Opuntia ficus-indica* cladodes: role of process parameters on hydrochar properties. *Bioresour Technol* 247:310–318. <https://doi.org/10.1016/j.biortech.2017.09.072>
36. Dehkhoda AM, Gyenge E, Ellis N (2016) A novel method to tailor the porous structure of KOH-activated biochar and its application in capacitive deionization and energy storage. *Biomass Bioenergy* 87:107–121. <https://doi.org/10.1016/j.biombioe.2016.02.023>
37. Anas M, Gönel AG, Bozbag SE, Erkey C (2017) Thermodynamics of adsorption of carbon dioxide on various aerogels. *J CO₂ Util* 21:82–88. <https://doi.org/10.1016/j.jcou.2017.06.008>
38. Zhou X, Yi H, Tang X, Deng H, Liu H (2012) Thermodynamics for the adsorption of SO₂, NO and CO₂ from flue gas on activated carbon fiber. *Chem Eng J* 200–202:399–404. <https://doi.org/10.1016/j.cej.2012.06.013>
39. Wang L, Yang RT (2012) Significantly increased CO₂ adsorption performance of nanostructured templated carbon by tuning surface area and nitrogen doping. *J Phys Chem C* 116:1099–1106. <https://doi.org/10.1021/jp2100446>
40. Hao W, Björnerbäck F, Trushkina Y, Bengoechea MO, Salazar-Alvarez G, Barth T, Hedin N (2017) High-performance magnetic activated carbon from solid waste from lignin conversion processes. 1. Their use as adsorbents for CO₂. *ACS Sustain Chem Eng* 5:3087–3095. <https://doi.org/10.1016/j.egypro.2017.08.033>
41. Yue L, Rao L, Wang L, Wang L, Wu J, Hu X, DaCosta H, Yang J, Fan M (2017) Efficient CO₂ capture by nitrogen-doped bio-carbons derived from rotten strawberries. *Ind Eng Chem Res* 56:14115–14122. <https://doi.org/10.1021/acs.iecr.7b02692>

Publisher's Note Springer Nature remains neutral with regard to jurisdictional claims in published maps and institutional affiliations.